INL/EXT-19-53710
Revision 0

Design of a Benchtop Fiber-optic Based Photothermal Radiometry System

Zilong Hua, Robert Schley, Zain Karriem, Austin Fleming, Zachary Thompson, Colby Jensen, and David Hurley

April 2019

The INL is a U.S. Department of Energy National Laboratory operated by Battelle Energy Alliance

INL/EXT-19-53710
Revision 0

Design of a Benchtop Fiber-optic Based Photothermal Radiometry System

**Zilong Hua, Robert Schley, Zain Karriem,
Austin Fleming, Zachary Thompson, Colby Jensen, and David Hurley**

April 2019

**Idaho National Laboratory
Idaho Falls, Idaho 83415**

http://www.inl.gov

**Prepared for the
U.S. Department of Energy
Office of Nuclear Energy
Under DOE Idaho Operations Office
Contract DE-AC07-05ID14517**

INTENTIONALLY BLANK

EXECUTIVE SUMMARY

Thermal transport properties of nuclear fuels, i.e., thermal conductivity and diffusivity, are critical parameters in the thermal design of a nuclear reactor. It is well known that thermal transport properties change temporally and spatially due to dynamic microstructural evolution as a result of neutron irradiation. A real-time instrument to monitor the local thermal property change, which can survive the harsh in-pile environment, will give researchers unprecedented access to fuel behavior during irradiation. Laser-based photothermal techniques are an ideal candidate to accomplish this specific task because of the remote, non-contact, and non-destructive features. In this report, we present the progress in the development of a benchtop photothermal radiometry (PTR) system to measure the thermal diffusivity of solid samples, and the preliminary design of a fiber-based PTR instrument to measure the real-time, in-pile thermal diffusivity of nuclear fuels.

The PTR technique measures the local temperature response from a modulated heat source by detecting the sample radiation heat flux. Initially, a well-developed thermal wave analytical model was fit to the data to obtain the thermal diffusivity. However, systematic errors from diffraction effects and non-linearity issues resulted in thermal diffusivity measurements higher than literature values. These effects have been studied and an improved analytical model has been developed accounting for these physics. A procedure for optimizing measurements from the benchtop system has been provided. Based on these studies and results, a fiber-based system has been designed to enable remote application as required for in-pile measurement applications.

INTENTIONALLY BLANK

CONTENTS

FIGURES

TABLES

ACRONYMS

A	Airy disk function
AC	alternating current, the periodic portion of the signal in this report
c	the speed of light
D	thermal diffusivity
d	sample thickness
DC	direct current, the non-periodic portion of the signal in this report
d_{Airy}	diameter of the diffraction Airy disk
d_{lens}	diameter of a lens
f	modulation frequency of the heating laser
f_{lens}	focal length of a lens
FWHM	full width half maximum
f#	f-number, the ratio of the focal length and diameter of a lens
h	Planck constant
IR	Infrared
k	thermal conductivity
k_b	Boltzmann constant
L	Spectral radiance
LN_2	liquid nitrogen
L_{th}	thermal diffusion length
NA	numerical aperture
PTR	photothermal radiometry
P_0	heating laser power/intensity
R	responsivity of the detector
r	cylindrical coordinate
r_{max}	measurement scan distance
Rs	heating laser spot radius (Gaussian)
S	detector output
s	Hankel transformation variable
S_1	object distance (between the sample and the lens)
S_2	image distance (between the image and the lens)
T	temperature
TW	thermal wave
z	cylindrical coordinate
λ	wavelength of the signal
Ω	solid angle
ω	angular frequency
Δr	distance between the heat source and the detection location

INTENTIONALLY BLANK

Design of a Benchtop Fiber-optic Based Photothermal Radiometry System

1. INTRODUCTION

In-pile measurement of changes in thermal transport properties of nuclear fuels and materials has become an intense area of research in recent years due to the availability of advanced measurement techniques and a strong emphasis of understanding fundamental material behaviors. While the behaviors of the nuclear fuels and performances of the reactor are directly related to the neutron irradiation-induced thermal transport property change, the harsh and complicated environment has been the main obstacle to performing in-situ measurement and collecting real-time experimental data that can significantly boost computational study and reactor design potential.

Laser-based photothermal techniques use an intensity-modulated laser beam to generate a local, transient temperature field in the sample. With the knowledge of the heating condition and the real-time measurement of the corresponding temperature field, the sample thermal transport properties can be extracted by solving the inverse problem. The non-contact and non-destructive advantages have made it one of the leading candidates for in-pile thermal property measurement of nuclear fuels. The photothermal radiometry (PTR) technique uses the infrared (IR) radiation heat flux from the sample surface to measure temperature response, and has the additional advantage compared to other photothermal techniques of being relatively insensitive to the surface preparation and condition variations. Meanwhile, the spatial resolution of PTR measurements can be on the order of ~0.05mm-3mm allowing flexibility to make local to bulk scale measurements possible.

In this work, the methodology, design and testing of a benchtop PTR system is presented, which has been used to measure the thermal diffusivity (D) of a set of standard samples in the range of $0.6\times10^{-6}m^2/s$ to $65\times10^{-6}m^2/s$ (D of typical nuclear fuels is in the range of $1\times10^{-6}m^2/s \sim 10\times10^{-6}m^2/s$). With the ultimate goal of in-pile measurement, the benchtop system was first built and tested to provide a well-studied, standard system to explore the critical parameters of the more advanced fiber system design to follow. Challenges associated with the testing measurements include lens-induced diffraction and non-linearities stemming from radiation heat emission. These challenges can cause important systematic errors such that they have been studied through an extended analytical model and using optical ray-tracing software ZEMAX. With optimization of experimental design and measurement procedure, the systematic errors from these sources have been reduced successfully. The experience and knowledge obtained from the benchtop system have been used to guide the preliminary design of a fiber-based PTR system. The design of the fiber-based PTR system is detailed in the last section of this report.

2. THEORY OF PTR THERMAL DIFFUSIVITY MEASUREMENT AND BENCHTOP SYSTEM

2.1 Thermal-wave Solution

If a sinusoidal heat flux with a Gaussian spatial distribution (radius Rs, intensity P_0, and the modulation frequency (f) is applied on a semi-finite bulk sample, from the thermal diffusion equation and boundary conditions in the cylindrical coordinates (r, z)

(1)

(2)

(3)

the expression of the temperature (T) field on the sample surface can be derived through Hankel transformation (variable s) as [1]

(4)

where ω is the angular frequency (ω=2πf), and k and D are the sample thermal conductivity and diffusivity, respectively. As the temperature field has a wave-form expression, it is also called a thermal wave (TW) with "AC" and "DC" components. As can be seen, the phase profile (the second exponential term) only contains D, but the amplitude profile also contains k. In practice, the measurement of the absolute amplitude is influenced by difficult to accurately define parameters such as, detection and heating spot sizes, surface conditions affecting emissivity and characteristics of detection, e.g. spectral sensitivity. Therefore, the phase profile (with respect to the distance between the heat source and the detection location, Δr) is commonly used to extract D. The TW length, or thermal diffusion length (L_{th}), is

defined as . *Included in both amplitude and phase term,* L_{th} is the critical length scale in the TW

measurements. The comparison between L_{th} and other length scales (e.g., sample size, heat source spot size, etc.) directly determines the measurement spatial range, sensitivity on different experimental parameters, and measurement accuracy.

2.2 Benchtop System and Preliminary Test

In the benchtop PTR system, a 405-nm wavelength heating laser (Cobolt 06-MLD) is used as the heat source. The intensity of the laser beam is modulated into sine-wave by a waveform generator (Stanford Research Systems Model SR345) that controls the peak-to-peak AC amplitude, DC offset, and modulation frequency. The laser beam is lens-focused, and the radius of the spot on the sample surface is ~80μm. A single lens (one-lens design) is used to collect the infrared (IR) radiation and image due to its relatively simple alignment requirement. An IR lens (Edmund Optics EO-87-954, focal length 200mm, diameter 50mm) is used to collect the radiation heat flux into a LN_2-cooled IR detector (InfraRed Associate Inc., MCT-13-0.0.25) with an integrated amplifier. A lock-in amplifier (Stanford Research System SR830) is used to improve the signal-to-noise ratio and extract the phase profile from the signal. The positions of the IR lens and detector are fixed during the measurement, and the laser is mounted on a set of motorized stages (Newport UTM100CC1DD) that can move in both horizontal and vertical directions to accomplish the spatial scan. The system design diagram, actual benchtop setup, and a set of the spatial scan phase profile (single frequency and multi-frequency) are shown in Figure 1 and Figure 2.

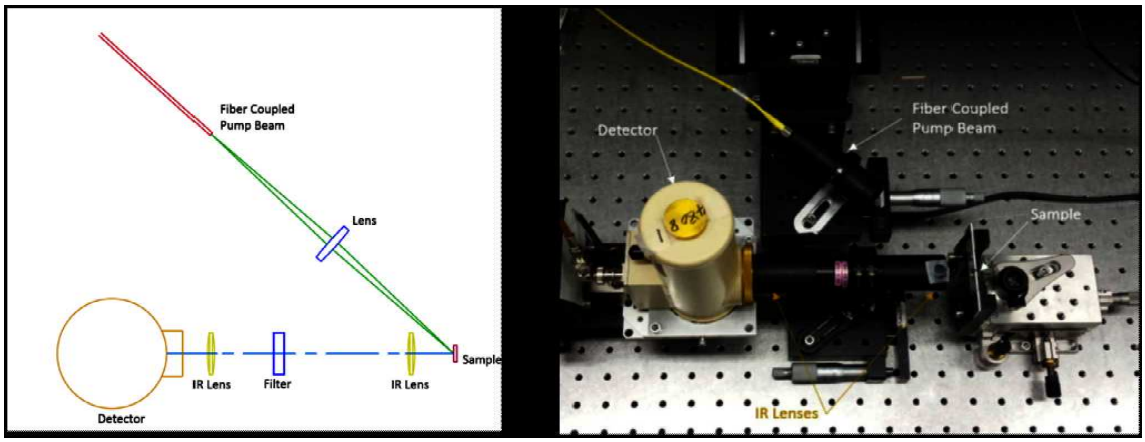

Figure 1. The design diagram and actual picture of the benchtop PTR system.

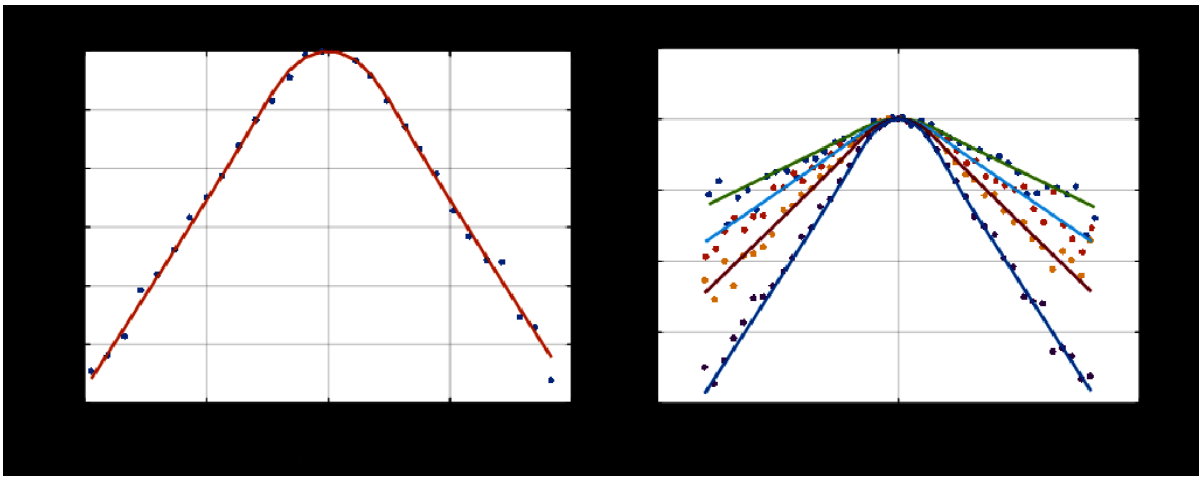

Figure 2 An example of the experimental data (left: single frequency; right: multi-frequency).

In order to improve the measurement accuracy, the phase profiles at multiple frequencies are collected to solve for D through a fitting process. However, systematic error was observed on relatively low-D materials ($D < 10\times10^{-6}m^2/s$), which tends to overestimate D. This overestimation increases with the modulation frequency and laser power output to up to a factor of 3 in extreme cases. One example on a standard sample with relatively low D, pyroceram, is given in Table 1. An approximately 120% overestimation (i.e., a factor of 2.2) was obtained in the measurement with 40Hz modulation frequency and ~80mW heat flux absorbed by the sample.

Table 1. Experimental data from thermal diffusivity measurements on pyroceram in units of $10^{-6}m^2/s$ illustrating biases due to diffraction and non-linearity effects. The measured difference from the reference value is ~120% in the worst case (40Hz, 80mW).

P f	5Hz	10Hz	20Hz	40Hz	Literature value is 2
20mW	2.05	2.15	2.42	2.66	
40mW	2.23	2.43	2.62	3.11	
80mW	2.26	2.54	2.73	4.41	

From previous studies [2,3], the primary reasons that cause the overestimation have been identified as the diffraction effect from the lens collecting infrared emission to the detector and non-linear behavior of radiation heat flux (detector signal) in relation to temperature rise on the sample surface. Although valuable insights have been provided to explain the phenomena, the related physics were investigated to understand their impacts for this setup from physical setup to data analysis.

In the next sections, we will present experimental and simulation studies focusing on analyzing the behaviors of the diffraction effect and non-linearity issue, and how they influence the measurement results.

2.3 Diffraction Effect

Diffraction occurs when a wave propagates through a small aperture or travels through a medium with a spatially varying index of refraction. It changes the wave propagation path and phase velocity. Thus, when the wave arrives at the "focal plane," the constructive and destructive interferences will redistribute the wave energy and form a diffraction pattern.

In the lens-based PTR system, the diffraction effect arises from the propagation of the radiation heat flux through the IR lens and causes the formation of the certain interference pattern on the detector plane. The interference pattern is approximated as an Airy disk, which is caused by focusing collimated light (plane wave) through a perfect lens with a circular aperture. An Airy disk has a bright center region and an alternative light-and-dark "ring structure," (as in Figure 3) and the spatial distribution of its intensity on the focal plane can be described as

(5)

where λ is the heat flux wavelength, and f_{lens} and d_{lens} are the focal length and diameter of the lens, respectively. In reality, the diffraction pattern is not strictly an Airy disk because of two primary differences. First, the incident wave is not a plane wave (far-field source), but irradiated from a point source (near-field). Second, the incident wave is not monochromatic but is composed of many wavelengths. While the latter issue may be approximated by superposing diffraction from all wavelengths weighted by spectral radiance, the former assumption has been evaluated using optical simulation to give a quantitative description.

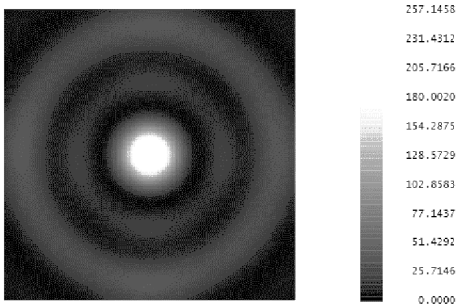

Figure 3.An Airy disk generated by ZEMAX.

The software ZEMAX uses ray tracing physics to model optical components and system designs (models can be downloaded from the vendor websites) to predict wave propagation paths. An example of the one-lens PTR system (with magnification of 1) with radiation from a point source focused by a lens, and the corresponding diffraction pattern, are given in Figure 4. The resulting PTR diffraction pattern has a similar geometry to the Airy disk with a solid circle-ring structure. In addition, by measuring the size of the center circle, the diameter of the PTR diffraction is larger than the values calculated by *Equation (5)* by a factor of approximately 2 (details are given in Table 2). Considering the one-lens system has an imaging formula as

(6)

where S_1 and S_2 are the object distance and image distance, respectively. Both S_1 and S_2 are larger than the f_{lens} by a factor of 2. Based on these observations, the distances are proposed to be used to replace f_{lens} in *Equation (5)* and make the equation still valid or reasonable enough to describe the diffraction pattern in PTR system. In order to prove it, ZEMAX simulation is used to obtain the diffraction pattern diameter of a system with the magnification = 2 (i.e., $S_1/S_2=2$). The results are summarized in Table 3. As can be seen, the diffraction pattern diameter reduces with a reduced S_2. As a matter of fact, by replacing f_{lens} by S_2 in *Equation (5)*, the predicted diffraction pattern diameter is always close to the simulation result with a difference of ~20%. With these similarities, we refer to the PTR diffraction patter also as an Airy disk for simplification reasons.

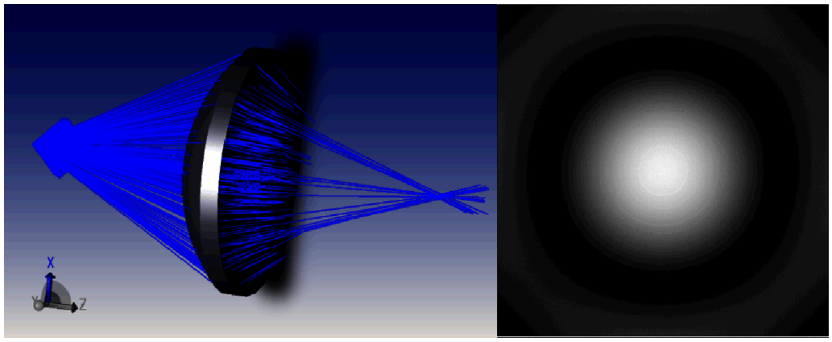

Figure 4 ZEMAX simulation of the one-lens system and the diffraction pattern.

Table 2. Airy disk diameter from ZEMAX simulation with different wavelengths.

Lens: EO-87-954 (f_{lens}=100mm, d_{lens}=100mm): Source at 200mm, detector at 200mm			
λ [μm]	Airy disk diameter [mm]		Factor (Z/A)
	Analytic (A) (far-field)	Zemax (Z) Source at 200mm from lens	
3.0	0.0146	0.0323	2.2
4.0	0.0195	0.0420	2.2
5.0	0.0244	0.0505	2.1
6.0	0.0293	0.0565	1.9
7.0	0.0342	0.0635	1.9
8.0	0.0390	0.0687	1.8
9.0	0.0439	0.0749	1.7
10.6	0.0517	0.0859	1.7

Table 3 Simulation results of diffraction pattern diameter with the magnification = 1 and 2.

Lens: EO-89-615 (f_{lens}=25mm, d_{lens}=50mm)			
	Airy disk diameter [mm]		
S_2/S_1	50mm/50mm	37.5mm/75mm	Far field (use S_2)
magnification	1	2	2
λ=7μm	0.0265	0.0152	0.0128
λ=8μm	0.0267	0.0166	0.0146
λ=9μm	0.0283	0.0184	0.0164
λ=10μm	0.0370	0.0207	0.0183

As shown in Figure 4, most of the energy is contained in the center area of the Airy disk, and, thus, d_{Airy} is expected to be used as the characterization length scale of the diffraction effect. The comparison of d_{Airy} and L_{th} are also expected to be the criterion of how much the diffraction effect influence the TW and, thus, the total signal. To investigate, a comparison of experimental results of pyroceram and Al_2O_3 is

given in Table 4. Assuming the temperature rise of the detection location is not obviously different from room temperature, from Wein's displacement law, the peak wavelength (i.e., the maximum contribution in IR heat flux) is ~10μm, and the corresponding d_{Airy} is ~80μm. The comparison between L_{th} and d_{Airy} shows a trend that the D overestimation becomes more obvious when L_{th} is shorter than 250μm, or three times d_{Airy} (Table 4, in bold). This conclusion is confirmed by testing with an additional adjustable aperture located in front of the IR lens to modify the effective lens diameter and thus d_{Airy} (details given in Table 4). It is interesting to point out that this quantitative relationship matches previous findings [4], in which the TW propagation was found influenced by the backside of the sample if the sample thickness is less than three times of L_{th}.

Table 4. Experimental results on pyroceram and Al_2O_3, with the comparison of d_{Airy} and L_{th}.

Sample	f	D(exp) [$10^{-6}m^2/s$]	L_{th} [μm]	d_{airy}/L_{th}
Pyroceram ($D=2\times10^{-6}m^2/s$, d_{Airy}=~80μm)	5Hz	2.05 (+2.5%)	357	4.46
	10Hz	2.15 (+7.5%)	252	3.15
	20Hz	2.42 **(+21%)**	178	**2.23**
Al_2O_3 ($D=12.5\times10^{-6}m^2/s$, d_{Airy}=80μm)	20Hz	12.8 (+2.4%)	446	5.58
	40Hz	13.1 (+4.8%)	315	3.94
	80Hz	14 **(+12%)**	223	**2.79**

Sample	Aperture	D(exp) [$10^{-6}m^2/s$]	d_{Airy} [μm]	d_{airy}/L_{th}
Pyroceram ($D=2\times10^{-6}m^2/s$, f=10Hz, L_{th}=252μm)	100%	2.23 (+11.5%)	80	3.15
	50%	2.43 **(+21.5%)**	160	**1.58**
	25%	2.61 **(+30.5%)**	320	**0.79**

In order to quantitatively describe this relationship, the basic TW model has been extended to consider both the diffraction effect and non-linear response of the received signal to the temperature change in the analytical solution in the next section. Other important features such as the non-linear detector responsivity and limited detector sizes are also included. By using this improved model, the distributions of diffraction and TW at different frequencies are presented in Figure 5(a). The sample material is set as Pyroceram, with the heating laser modulation frequency set at 10Hz, 20Hz, and 40Hz. All parameters in the model are set to match the actual experiment conditions. The amplitude of distributions is normalized with those at 10Hz. As can be seen, comparing with the diffraction distribution that is decided by the measurement setup and remains the same at all frequencies, both the TW distribution full width half maximum (FWHM) and amplitude get smaller at higher frequency due to the reduction of L_{th}. This observation explains why the TW disappears faster in the spatial domain with an increasing measurement frequency, and the diffraction effect dominates the total signal and corresponding phase profile. Meanwhile, an extreme case at high modulation frequency shows that, if L_{th} is much smaller than d_{Airy}, the phase nearly becomes a constant and is independent of the separation of the heating and detection locations (as Figure 5(b) shows), leading to the model predicting D approaching infinity.

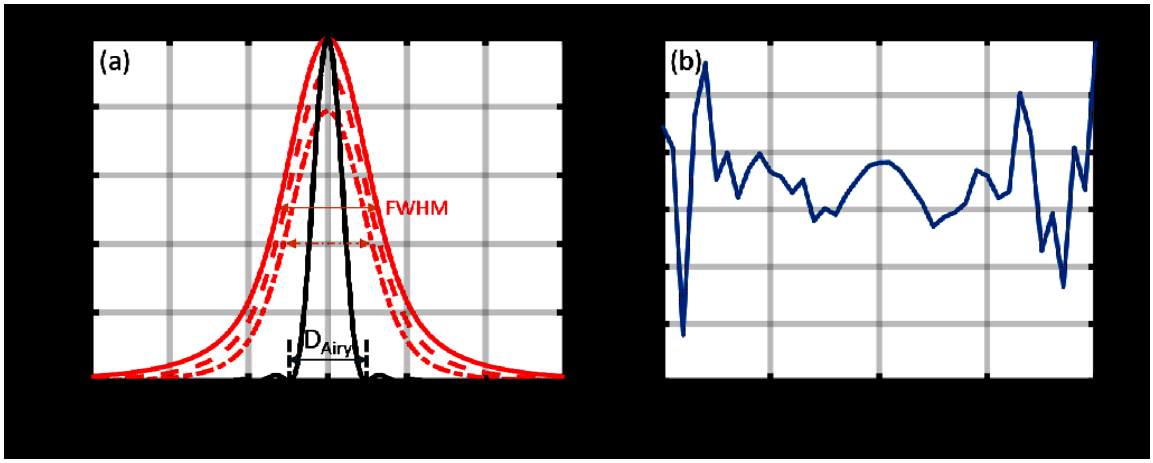

Figure 5. (a) Amplitude comparison between Airy disk and TW at different frequencies (modeling work). (b) The phase profile of pyroceram at 1KHz. The diffraction effect dominates the signal and phase profile is nearly independent to the heat source-detection separation here.

2.4 Non-linearity Issue

Besides the diffraction effect, a sample surface temperature rise can also contribute to systematic errors, i.e., D overestimation, by causing a non-linearity issue and chromatic aberration related to focal plane shift. As the index of refraction of the IR lens in this setup does not change with λ significantly (within 2%), the non-linearity issue is the primary focus of this section. The chromatic aberration will be briefly discussed in the next section.

When analyzing the heat flux signal and resulting phase profile to extract D from the thermal-wave model, the heat flux signal is assumed to be in phase with temperature, i.e., the heat flux and temperature have a linear relationship. However, based on Planck's law, the spectral radiance (L) (linear relationship to measured radiation heat flux) is related to temperature following the non-linear equation as

(7)

where h, c, and k_b are Planck constant, the speed of light, and Boltzmann constant, respectively. The difference between the phases of spectral radiance and T is negligible with a small variation in temperature. However, it rapidly becomes problematic when the temperature rise is not negligible compared to the ambient temperature. Using *Equation 7*, the plot of dL/dT with respect to T (in the range of 275K-475K) at several λ are given in Figure 6. As can be seen, dL/dT is more non-linear at shorter λ. Based on Wein's displacement law, the non-linearity issue is more important at higher T because short λ radiation weighs more heavily in the total signal.

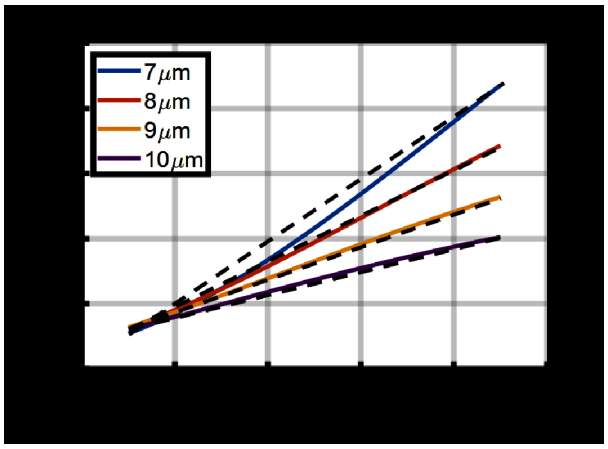

Figure 6. dL/dT change with T in the range of 275K-475K.

To reduce the non-linearity issue, the temperature rise needs to be maintained under a threshold value. Validated by our improved model and experiments, the threshold T_{DC} rise and corresponding laser output powers absorbed by the sample surface are summarized in Table 5 for standard samples. In actual measurements, if a prior estimation of the sample thermal properties is available, the non-linearity issue can be safely avoided by selecting the power settings following this table. With an unknown sample, an iterating measurement procedure with D obtained from a test run can still reduce or avoid the non-linearity induced biasing. The details are included in the following chapter.

Table 5 Recommended T_{DC} rise and laser power absorption on reference samples.

Sample	Thermal Diffusivity [$10^{-6}m^2/s$]	T(DC) [K]	Output power [mW]
Pyrex	0.6	2	5
Pyroceram	2	5	10
Al_2O_3	12.5	10	40
Poco graphite	65	10	200

2.5 Recommendations of the Optics and System Design

In previous sections, important systematic errors were analyzed in relation to addressing biasing causing overestimation of D. In this section, the procedure to reduce such errors are detailed, with perspective of the optics selection and system design.

1. Lens selection

Equation (5) indicates a linear relationship between the d_{Airy} and f# (f_{lens}/d_{lens}) of the lens. A lens with a smaller f# can reduce d_{Airy} and thus the diffraction effect at a given f, or leave more space to increase f and improve the measurement accuracy. In addition, a smaller f# can increase the solid angle of the radiation heat flux reception and signal level. The primary disadvantage of a smaller f# is that also obstructs access from the heating laser beam, reducing the incident angle beam to the sample surface. This effect results in causing the heating region spatial profile on the sample surface to be further asymmetric and different from the Gaussian distribution assumed in the analytical model. It will lead to a phase profile asymmetry at a higher f when L_{th} approaches Rs.

Another important parameter during the lens selection is the index of refraction variation with respect to the IR λ. The index of refraction represents the ability of the lens to change the path of the incident light waves (i.e., focus the incident waves). As the index of refraction is λ dependent, the lens will focus

waves composed by different λ to different focal plane, which is defined as chromatic aberration. On the other hand, the detector receives radiation heat flux for all λ without differentiation. The phase difference introduced by unfocused components inevitably cause errors to the signal output. The details are more complicated and will not be given here. Generally, the germanium lens has more consistent index of refraction than the ZnSe lens and should be selected.

2. Two-lens system

As described previously, d_{Airy} can be reduced by shortening S_2. But as a compromise, the system will have a larger magnification and, thus, lower spatial resolution. It is possible to reduce d_{Airy} without sacrificing the measurement resolution by using a two-lens system, of which S_1 and S_2 both depend on f, and with identical lens, $S_1=S_2=f$ and the system has a magnification = 1. A two-lens system (f_{lens}=100mm for both lenses) simulated by ZEMAX gives the d_{Airy} of 0.0535mm (λ=10μm), smaller than d_{Airy} of the one-lens system (0.085mm). The comparison of the simulated Airy disks is given in Figure 7.

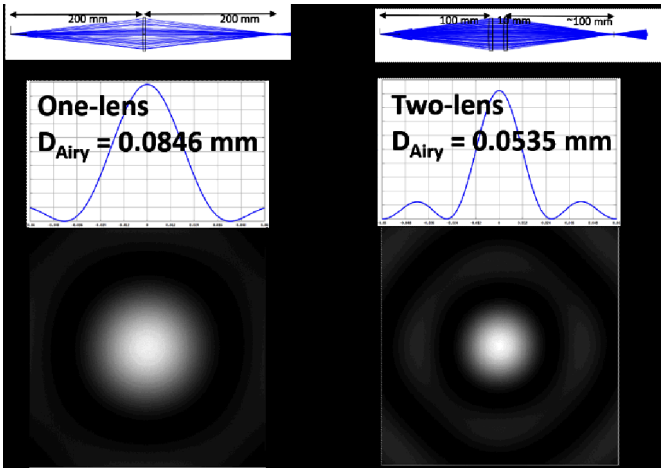

Figure 7. Simulated Airy disk from the two-lens and one-lens systems. The lenses in both systems all have f_{lens}=100mm, and the system magnifications are both 1.

3. The use of bandpass filters

The bandpass filter can restrict the range of the heat flux wavelength received by the detector. In theory, it should nearly eliminate the chromatic aberration, and can help describe the diffraction pattern and non-linear response in a more accurate manner so the signal can be more closely predicted and fit by the extended model accounting for these effects. However, two primary parameters need to be considered in the bandpass filter selection: center wavelength and bandwidth. As shorter λ have a more obvious non-linearity issue, but longer λ have a more obvious diffraction effect, the selection is essentially a tradeoff between these two negative effects. Similarly, the bandwidth selection is a tradeoff between improved signal level and acceptable chromatic aberration. As both parameters depend on specific experimental conditions, a detailed discussion will not be given in this section.

2.6 Extended Analytical Model

An improved analytical model that describes the received signal by the detector and corresponding phase profiles is derived based on the study and discussion in previous sections. While Planck's law and the TW solution have been described in good detail, Airy disk function (A) from a point can be described

as *with* S_2 used instead of f_{lens}. The heat flux reception of the detector output (S) at a single wavelength

(λ_0) is thus calculated as $S(\lambda_0)=\Omega\times L(T, \lambda_0)\times A(r)\times R(\lambda_0)$, where $R(\lambda_0)$ is the responsivity of the detector at wavelength λ_0, and Ω is the solid angle. The L can then be Taylor expanded as

(8)

and S can be calculated in the Hankel space as the convolution of L and A, as [5,6]

(9)

where det(r) describes the detector geometry. Ω is omitted, as it does not contribute to the phase profile. By integrating the $S(\lambda_0)$ at the wavelength range of the detector, the total signal output S (AC component, which really matters in the measurement) can be obtained. A set of comparisons between the modeling prediction and experimental results (power absorption is ~38mW) on pyroceram are given below in Figure 8. While the TW model can correctly predict the experimental phase profile at 1Hz (Figure 8(a)), it fails to predict phase profile at 20Hz (Figure 8(b)); and the improved model correctly predicts both, including the extensive phase deformation at 20Hz.

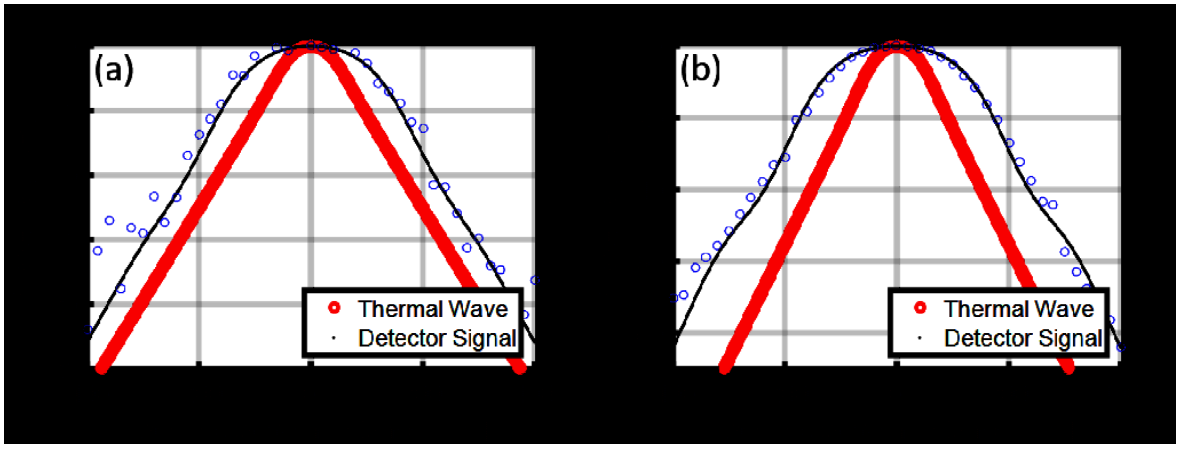

Figure 8. Phase profile comparisons: thermal wave model (red), extended model accounting for diffraction effects (dark), and experimental results (blue dot).

3. RECOMMENDED MEASUREMENT PROCEDURE

Although the extended model has been developed, the simpler, "thermal wave only" model is still recommended for practical measurement from well-controlled experiments for several reasons. The most important reason is the addition of several parameters to the model, which contribute to overall uncertainty of the measurement. For the extended model to provide high accuracy, it is necessary to have the critical parameters measured or determined separately, which may be difficult or impractical in some cases. Spectral emissivity is an example of a parameter that is difficult to quantify sufficiently. As it determines the amplitude of the emission heat flux and laser power absorption, the spectral emissivity is

directly related to the signal amplitude and sample temperature. However, it is well known that the spectral emissivity depends on numerous factors from the material composition to specific surface preparation. Accurate emissivity measurement is a challenge for experimentalists in the best of circumstances. Another drawback to relying on the extended model is longer required measurement time. Roughly, the extended model requires 20-50 times longer to perform a single fitting iteration compared to the simpler model. If initial input estimates are far from the best-fit results, the duration of the fitting process is exacerbated.

Importantly, the extended model aids in proper design of the measurement to allow use of the simpler TW model. The essential design criteria are the comparisons between the following length scales: thermal diffusion length (L_{th}), Airy disk diameter (d_{Airy}), sample thickness (d), the Gaussian radius of the heating laser spot (R_s), and the scan distance (r_{max}). In the following analysis, L_{th} is used as the primary tool for demonstrative purposes.

In order to reduce the diffraction effect, L_{th} needs to be at least 3 times longer than d_{Airy}. This rule of thumb drives lens selection with an appropriate f#. It also sets the upper bound of the measurement frequency that can ensure the minimum L_{th}. The lower bound of the measurement frequency is related to d. In order to make the semi-infinite geometry assumption valid, L_{th} needs to be shorter than ~1/3 of d. In the extreme case, if a thin material with high thermal diffusivity (e.g., silicon or poco graphite with thermal diffusivity higher than $60\times10^{-6}m^2/s$) is measured, the described upper bound for f may be below the described lower bound for f, and, thus, no optimal f exists. To deal with this problem, a model for a limited thickness has been derived. Parameters r_{max} and R_s are related to L_{th} through the measurement sensitivity. A higher sensitivity to thermal diffusivity can improve the measurement accuracy. The rule of thumb is for r_{max} to be 150%-200% of L_{th}, and 400% of R_s (detailed explanation can be found in [7]).

Following the criteria listed above, the recommended measurement procedure is:

1. During the system buildup, select the lens with a low (f#). With the same specification parameters, a two-lens system has a smaller d_{Airy} than the one-lens system, and, thus, is preferred.

2. Calculate d_{Airy} using . *The minimum L_{th}* is determined to be $3\times D_{Airy}$, which then gives the heating

   laser frequency in the test measurement, as *(f can be further reduced by 50% to better avoid*

   diffraction effect).

3. Perform a test measurement with an estimated D. D can be briefly estimated from the material type, i.e., $1\text{-}10\times10^{-6}m^2/s$ for oxides, and $10\text{-}50\times10^{-6}m^2/s$ for metals/silicide.

   If R_s can be measured, make sure L_{th} is 200%-250% of R_s. r_{max} should be at least 150% of L_{th}. Longer scan distance is recommended while providing sufficient signal-to-noise ratio (i.e., the AC signal amplitude from the lock-in amplifier should be higher than a threshold value).

   The laser power in the test measurement needs to be controlled to avoid the non-linearity issue. The recommended heating laser power can be found in Table 4 for estimated thermal diffusivity. In the

worst case that no sample information is available, perform the test measurement at 20Hz with the laser power of 20 mW and scan distance of 400 μm.

4. Extract D and R_s from the test measurement by using the TW model. With the preliminary measured thermal diffusivity, all parameters in Step 3 can be updated for a second iteration of measurement, which is performed at multiple frequencies to improve the accuracy of results.

Following this procedure, we did blind measurements on the reference samples, of which D is summarized in Table 6. As can be seen, a < 10% measurement difference from literature values has been achieved.

Table 6. Experimental results of standard samples following the optimized measurement procedure.

Sample	Measurement frequency	Measured D [$10^{-6}m^2/s$]	Reference D [$10^{-6}m^2/s$]	Difference %	L_{th}
Pyroceram	4Hz	2.04	2.00	2%	400 μm
Al_2O_3	7Hz	11.94	12.5	-4.5%	740 μm
Poco graphite	100Hz	68.95	64.6	6.7%	470 μm
Pyrex	1.6Hz	0.581	0.694	-16.4%	340 μm

4. FIBER-BASED SYSTEM DESIGN

With the detailed understanding gained from the free space optical system, a fiber-based system has been designed. The major modification to the fiber-based PTR system from the benchtop system involves the use of fiber optics to provide the guide for laser heating and collection of IR signal, as shown in Figure 9. Considering the sizes of the fiber core and cladding layer, the possibility of scanning a fiber relative to the other is impractical since separation distance is already relatively high for good signal-to-noise ratio needed for precise measurements and physically moving the fibers in a precise manner adds additional complexity to the design. Therefore, scanning heating frequency with a fixed spatial distance between heating and detection will be done instead of more typical spatial scanning at a fixed frequency, for related photothermal techniques. A similar optical fiber design has been reported for a different photothermal technique [8], from which, the most critical parameters to ensure good measurement accuracy have been identified as the heating beam fiber tip diameter and the distance between the heating and probe fiber tips. The design of both parameters needs to be related to the thermal diffusion length, discussed at length in previous sections of this report. One example of the previous experimental data of the frequency-domain scan measurement that covers a thermal diffusivity range of $1\sim35\times10^{-6}m^2/s$ is given in Figure 10 (i.e., SiO_2 and germanium, respectively). With a similar analytical model for thermal diffusivity extraction, the accuracy of the frequency scan measurements is comparable to the traditional spatial scan measurements [9] (3-5% in the plot).

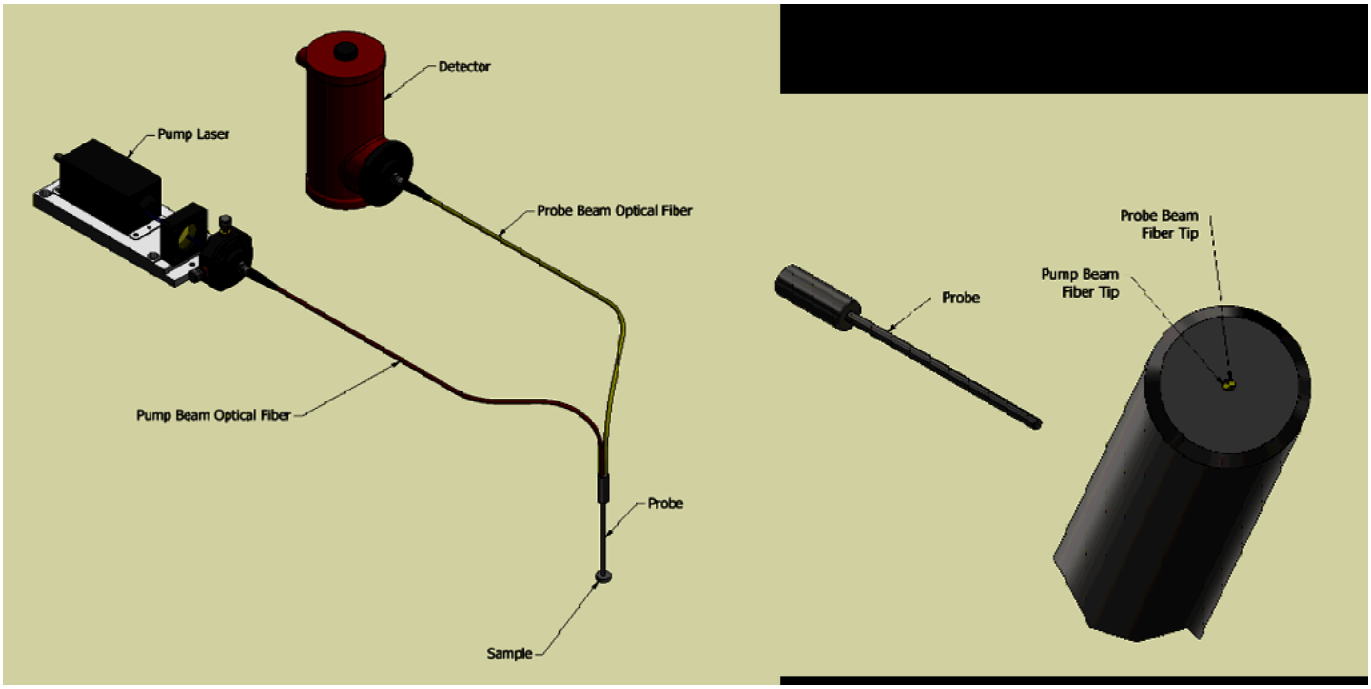

Figure 9. Design diagram of the fiber-based PTR system. System components are currently being procured and assembled. The dual fiber probe and frequency scanning approach are crucial novel aspects to this system.

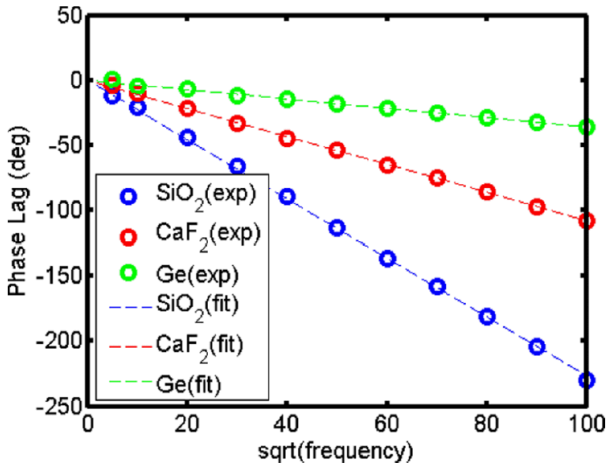

Figure 10. Experimental data of frequency-domain scan thermal wave measurements.

The design of the fiber-based PTR system follows the conclusions obtained from the benchtop system studies documented in this report. The maximum scan distance in the benchtop system is replaced by the center-to-center distance between the heating and probe fiber tips, and the heating spot radius is closely replaced by the heating fiber tip radius. As concluded from the previous chapter, the distance between tips, thermal diffusion length, and the heating fiber tip radius, is recommended to have a length ratio of 4:2.5:1. However, since the thermal diffusion length changes during the frequency modulation and a larger frequency range can improve the measurement accuracy, the length ratio of the distance between fiber tips and heating fiber core radius should be approximately 10:1. On the other hand, the small core radius will influence the signal reception, which requires the fiber to have a low transmission loss to

compensate. The Thorlabs fiber FG105UCA was selected as the heating fiber for its small core diameter of 105 μm and high transmission as 99% per meter. In addition, this fiber has a relatively low numerical aperture (NA=0.22), which can help reduce the heating spot radius. The probe fiber was selected as the Thorlabs MF11L1, which is made of InF_3 and has a core diameter of 100 μm. The probe fiber has a relatively large working wavelength range up to 5 μm, at which the transmission can still be kept at 90% per meter. The coating diameters of FG105UCA and MF11L1 are 250 μm and 287 μm, respectively, and, thus, the center-to-center distance between the heating and probe tips is, if the two fibers are bound to each other by the outside of the coating, ~530 μm, which is ~10 times longer than the heating fiber radius (52.5 μm), reaching the design requirement.

One parameter that may need to be adjusted after experimentation with a prototype is the working distance between the fiber tips to the sample surface. As can be seen in Figure 9, a cylindrical rim is designed on the edge of the fiber probe to keep the working distance between the tips to the samples consistent in every measurement. In our initial design, this distance is designed to be 10 μm to increase radiation heat flux reception and reduce the diffraction effect. From Planck's law and Wein's displacement law, the heat flux at room temperature peaks at the wavelength of 9-10 μm (the current fiber transmits well up to 5 μm). Due to few available options of fibers for IR applications, the working distance should be small to increase the solid angle and maximize signal collection. Based on the studies described previously, the non-linearity issue may become our primary challenge in this wavelength range, and a small modulation amplitude of the pump laser power will be used to minimize this effect. If a sufficient signal-to-noise ratio can be obtained through this system, but the non-linearity issue becomes problematic, the Newport polycrystalline fiber (Model# 76098) is an additional option that has a working wavelength up to 18 μm but a lower transmission of ~60% per meter.

The initial design specification for this system are components that will operate at room temperature. The specimen temperature could vary though its impacts on the fiber probe will need to be evaluated. The system is also designed to target specimens with thermal conductivity of nuclear fuels ranging from 0.1 to 30 W/m/K.

To date, all required system components have been procured or are in hand and fabrication of the custom fiber probe tip is underway. The fiber-based system will be set up and will begin testing for the remainder of this fiscal year to provide guidance to a final fiber-based design that will specifically target in-pile deployment (e.g. considering fiber lengths, temperature requirements of components, connectors, etc). The measurement model and fitting algorithm has been revised to work for the frequency-domain measurement, and preliminary experimental results are expected this fiscal year.

5. SUMMARY

Thermal transport properties of fuels play important roles in the nuclear reactor design. The real-time, in-situ measurement capability of fuels has become a strong need in recent years. The methodology, design, testing, and optimization of a benchtop PTR system to measure thermal diffusivity has been presented. Diffraction and non-linearity issues have been identified as the primary reasons for the observed systematic errors with detailed studies. Unique analytic models and experimental solutions have been derived and presented to mitigate associated impacts and enable advanced PTR measurements required for in-pile applications. The results of these studies with a free-space benchtop system and data analysis have contributed to a solid prototype design of a fiber-based system, which will be tested in the remainder of FY19. The conclusions and validation provided by these benchtop systems will then contribute to the final design and construction of mature fiber-coupled PTR system for in-pile measurement of thermal conductivity.

6. REFERENCES

[1] B-C. Li, S-Y. Zhang, "The effect of interface resistances on thermal wave propagation in multi-layered samples," *J. Phys. D*, **30**(10), pp. 1447-1454 (1997).

[2] J.F. Bisson, D. Fournier, “Influence of diffraction on low thermal diffusivity measurements with infrared photothermal microscopy,” *J. appl. Phys*., **83**(2), pp. 1036-1042 (1998).

[3] J.F. Bisson, D. Fournier, “The coupled influence of sample heating and diffraction on thermal diffusivity estimate with infrared photothermal microscopy,” *J. appl. Phys*., **84**(1), pp. 38-43 (1998).

[4] Z. Hua, H. Ban, “Thermal diffusivity measurement of focused-ion-beam fabricated sample using photothermal reflectance technique,” *Rev. Sci. Instrum*., **88**(5), 054901 (2017).

[5] A. Feldman, N. M. Balzaretti, “A modification of Angstrom’s method that employs photothermal radiometry to measure thermal diffusivity: application to chemical vapor deposited diamond,” *Rev. Sci. Instrum.*, **69**(1), pp. 237-243 (1998).

[6] S. Paoloni, D. Fournier, “Semi-empirical approach for the analysis of infrared photothermal microscopy,” *J. appl. Phys*., **92**(10), pp. 5955-5958 (2002).

[7] L. Fabbri, P. Fenici, “Three-dimensional photothermal radiometry for the determination of the thermal diffusivity of solids,” *Rev. Sci. Instrum.*, **66**(6), pp. 3593-3600 (1995).

[8] Z. Hua, H. Ban, D. Hurley, “The study of frequency-scan photothermal reflectance technique for thermal diffusivity measurement,” *Rev. Sci. Instrum.*, **86**(5), 054901 (2015).

[9] Z. Hua, H. Ban, M. Khafizov, R. Schley, R. Kennedy, D. Hurley, “Spatially localized measurement of thermal conductivity using a hybrid photothermal technique,” *J. appl. Phys*., **111**(10), 103505 (2012).